Strojniški vestnik - Journal of Mechanical Engineering 70(2024)7-8, 325-341
DOI:10.5545/sv-jme.2023.764
Original Scientific Paper
Received for review: 2023-08-17
Received revised form: 2024-02-22
Accepted for publication: 2024-03-01

Analysis and Research on Energy Consumption of a Non-Contact High-Efficiency Tunnel De-Icing Device

Hongwei Yan – Qi Chang – Hailong Niu – Guorui Wang – Pengyang Zhao – Bolong He
North University of China, School of Mechanical Engineering, China

To solve the problem of ice forming on the top of the tunnel and achieve more efficient and convenient de-icing, we designed a tunnel laser de-icing device. First, Solidworks software was used to create a 3D model of the laser de-icing device, namely the track module, the base platform, and the work platform. Then, ANSYS simulation software is used to simulate the process of laser de-icing. When the initial temperature of the icicle is -5 °C, -10 °C, -15 °C and -20 °C, the distance between the laser and icicle is 1.5 m, 2 m, 2.5 m, and 3 m, and the wind speed is 2 m/s, 3 m/s, 4 m/s and 5 m/s, respectively. The depth of 200 s of laser irradiation and the time of full penetration were simulated under three variables. It is concluded that the higher the initial temperature, the closer the distance and the smaller the wind speed, the lower the de-icing energy consumption. Finally, the experiment results are consistent with the simulation results, which further verifies the accuracy of the simulation. The laser de-icing detection device studied in this paper provides a certain theoretical basis and reference value for the application and development of intelligent de-icing equipment in tunnels.

Keywords: tunnel engineering, laser de-icing, energy consumption analysis, simulation analysis

Highlights

- *A non-contact laser de-icing inspection device is designed to automatically inspect, identify, and remove the icicle on the tunnel top wall on the track of the tunnel side wall.*
- *The simulation analysis of the laser de-icing process is carried out with ANSYS software, which lays a foundation for the subsequent experiment.*
- *A prototype of the laser de-icing inspection device was built. The device's de-icing energy consumption was tested by changing the initial icicle temperature, the distance between the laser and the icicle, and the ambient wind speed.*
- *The higher the initial temperature, the closer the distance, and the smaller the wind speed, the lower the de-icing energy consumption.*

0 INTRODUCTION

With the rapid improvement of science and technology, the railroad and highway businesses have ushered in a peak period of development [1]. At present, the routine maintenance of tunnels has become one of the key points of the overhaul of railroad [2] and highway facilities [3]. Due to the ageing of the tunnel's top and the emergence of cracks leading to water seepage from time to time, in alpine regions, the top wall of the tunnel is prone to condense into icicles [4]. This icicle will continue to increase with the continuous seepage of water, posing a serious threat to tunnel equipment and the safe operation of vehicles [5]. Therefore, removing the icicle from the tunnel roof wall has become the first task in the routine maintenance of tunnels [6].

Currently, there are two main solutions for dealing with ice and snow coverage in tunnels: anti-icing and de-icing [7]. Anti-icing measures are primarily used in areas with low ice-carrying capacity or where large-scale ice disasters may occur. They are applied during the initial stage of ice formation to prevent or reduce the accumulation of ice, thus avoiding serious ice disasters [8] and [9]. De-icing refers to the use of specific tools and methods to remove as much ice as possible. These methods are typically employed in localized areas after ice disasters or snowstorms [10]. Since the 1980s, the de-icing methods have developed from the initial rolling method and short-circuit heating method to 15 different de-icing technologies by 1998 [11]. In summary, de-icing technology can be divided into two categories: active de-icing technology and passive de-icing technology. Among them, active de-icing technology refers to the direct removal of ice by using external energy, such as thermal energy, electrical energy, mechanical energy, etc., usually including thermal de-icing technology [12], mechanical de-icing technology [13], and chemical de-icing technology [14], ultrasonic de-icing technology [15], microwave de-icing technology [16], and laser de-icing technology [17], which have the characteristics of fast response and high efficiency.

However, due to diminishing resources and a significant increase in energy consumption, particularly in refrigeration and related fields, the global energy sector is facing significant challenges. Within the de-icing technology domain, challenges such as high operating costs, complex system

*Corr. Author's Address: School of Mechanical Engineering, North University of China, Taiyuan, China, aweigeyan@nuc.edu.cn

maintenance [18], and significant energy requirements are prevalent.

Passive de-icing technology relies on the characteristics or design of the material itself and can achieve anti-icing or reduce ice adhesion without external energy. Common passive de-icing technologies include hydrophobic coatings [19], low-adhesion surfaces, and heating resistors [20], etc., are designed to reduce the adhesion of ice so that natural forces (such as gravity or air flow) can more easily remove the ice layer, are simple to maintain, and generally have lower maintenance costs and energy requirements [21], but in some cases In extreme weather conditions, the effect of passive de-icing technology may not be as significant as active de-icing technology, and there are great technical limitations. Among them, laser de-icing requires no contact with the surface of snow and ice, featuring extremely high precision in positioning and control [22]. It adapts to various snow and ice types, produces no pollutants, and is environmentally friendly and efficient. This also renders it a versatile and efficient solution [23].

Researchers carried out experiments on the long-distance removal of surface icing of materials by laser, using two different wavelengths of laser, 1060 nm and 694.3 nm, to remove the surface icing of six different materials, such as asphalt, brass, concrete, etc., and verified the feasibility of the method [24]. Lee [25] conducted simulation research and experiments on the propagation process of coin-shaped cracks generated under internal pressure after the interface between the ice cube and the substrate was irradiated by a laser beam during the de-icing process [26]. Long et al. [27] invented a de-icer that used microwave energy to remove ice from roadways. However, due to the poor heat absorption performance of road paving materials under the action of microwaves, the de-icing effect is poor, and the test results are unsatisfactory [28]. Loth et al. [29] published a study on aircraft ice protection systems and discussed a variety of de-icing technologies, including chemical, electrothermal and mechanical methods. Stolfi and Swift [30] published a study on wind turbine blade de-icing systems and discussed electric heating and coating technology. Hopstock [31] discovered that iron oxides have good absorption of microwave energy, and such oxides are abundant in taconite, so taconite was added to asphalt concrete, and one road was paved to conduct microwave de-icing experiments. Experimental results show that the new pavement material combined with taconite has greatly improved microwave absorption performance, significantly increased de-icing efficiency and can meet the requirements for rapid de-icing [32].

Xiao et al. [33] simulated the transient temperature distribution of the ice under laser irradiation as well as the thermal stress field using finite element software and analysed it by comparing the experiments with the results of the laser de-icing and the simulation. Researchers simulated and analysed the temperature and stress distribution on the surface of the ice body by using finite element analysis software to irradiate the ice with a laser [34] and [35]. Qi [36] discussed the icing situation on transmission lines, further studied the application of laser de-icing technology in high-voltage line de-icing, and proposed the theory of surface heat sources and body heat sources. Cheng et al. [37] made a systematic analysis of the principle of microwave de-icing in tunnels based on the microwave heating theory. According to the laws of thermodynamics, they derived the conduction equation inside the concrete after the microwave energy is converted into heat energy. At the same time, the thermal boundary conditions are given; under the given working conditions under the assumed conditions, the software is used to establish a tunnel microwave de-icing model for simulation calculations. By analysing the temperature distribution of the internal structure of the ice and the required heating time, the optimal microwave de-icing efficiency is obtained. [38]. Liu et al. [39] designed a laser from an optical perspective that can automatically adjust the spot diameter according to the distance between the laser and the ice. At the same time, they also measured the spot diameter, laser focal length, and the distance between the laser and the ice and analysed their relationship. Zhong [40] combined six aspects of electromagnetic thermogenesis theory, heat transfer theory, and fluid mechanics. They gave the quantitative calculation equation of the thermal effect of the laser, derived the transmission characteristics and characteristic parameters of common Gaussian beams in the atmosphere, developed a prototype of a de-icing machine, and carried out the corresponding experiments [41] and [42].

This paper proposes a new non-contact laser de-icing device for removing icicles from the roofs of tunnels. The device uses laser de-icing to remove ice faster and more efficiently without the use of chemicals or large amounts of energy, reducing the negative impact on the environment. It also uses non-contact technology that eliminates the need for physical contact with the ice surface, making it ideal for different types of tunnels. The structure and ice layer have high applicability. This paper provides

theoretical and data references for the research of environmentally friendly and efficient de-icing technology.

1 TUNNEL LASER DE-ICING PATROL UNIT STRUCTURAL DESIGN

1.1 Laser De-Icing Patrol Unit Overall Program Design

The overall assembly of the laser de-icing inspection device is shown in Fig. 1.

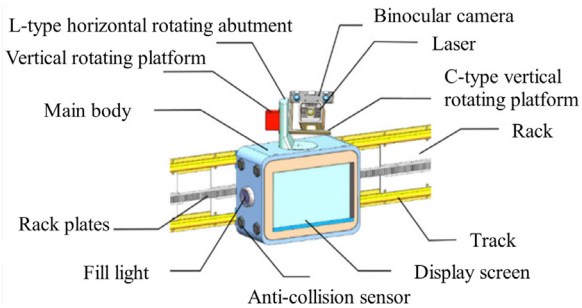

Fig. 1. Overall assembly diagram of laser de-icing inspection device

The designed de-icing inspection device's mechanical structure mainly consists of three parts: the tracking module, foundation platform, and working platform. The tracking module comprises the track, slider, rack plate, and rack; the base platform includes the power supply module and transmission module; and the working platform incorporates the connection module and specific working parts. This laser de-icing inspection device is designed to be independent of each component, ensuring that they do not interfere with one another. It is easy to disassemble [43], which facilitates subsequent maintenance and allows for structural optimization if needed [44].

1.2 Overall Assembly of Rail Module

The laser de-icing inspection device uses a rack and pinion for transmission. The rack needs to be fixed in the track module so that the base platform and the rack can maintain relative motion [45]. The overall assembly of the track module is shown in Fig. 2. The laser de-icing inspection device's track module utilizes a dual rail running mode to save materials. It involves applying several discontinuous rack plates fixed between the two rails. These rack plates are secured to the side wall together using bolts and rails. The rack itself is fixed on the platform, specifically on the rack plates.

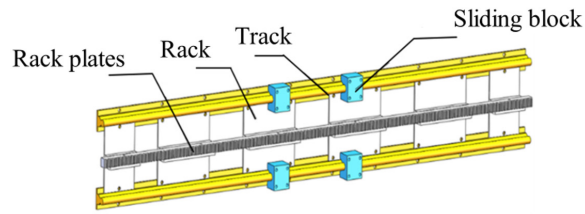

Fig. 2. *Overall assembly diagram of track module*

1.3 Design of the Base Platform for Laser De-Icing and Inspection Devices

Due to the different voltages required by the drive motor as well as the servo, the modular power supply method is used [46], and a double battery compartment design is carried out, using two batteries to power the drive motor as well as the servo respectively, as shown in Fig. 3a. The motor requires a higher voltage and a larger battery volume, so it goes into battery compartment 1. In contrast, the servo requires a smaller voltage and a reduced volume, so it goes into battery compartment 2. The two battery compartments open in opposite directions, and each has its own end cap for installation.

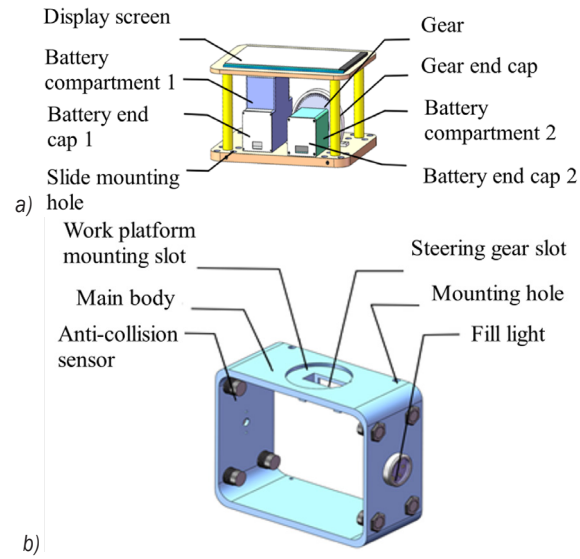

Fig. 3. *Schematic diagram of drive module structure; a) driving body, and b) protective shell*

The motor compartment is fixed on the lower surface of the abutment, and the motor is placed inside it. The motor is connected to the gear using the top wire, and the gear meshes with the rack through the square hole on the lower surface of the abutment. When the motor rotates, it drives the gear to rotate. Because the gear meshes with the fixed rack, the

torque generated moves the overall device. End caps are installed to prevent the gear from becoming entangled with the wire during rotation, thereby safeguarding the wire. Additionally, a display screen is installed on the top plate of the abutment. This screen can monitor and display real-time information such as the device's running speed, the temperature and humidity of the surrounding environment, and relevant parameters when the device encounters an obstacle in its running path, including the distance between the device and the obstacle.

The schematic diagram of the protective shell is shown in Fig. 3b. Due to the device's special working environment, situations like water leakage may occur from time to time. To prevent electrical wires and other energized devices from being affected by leaks and other circumstances in the external environment, the abutment is designed with an additional protective shell to prevent such occurrences. The protective shell takes the form of a shell to achieve the purpose of explosion-proofing and to protect the abutment surroundings. We added collision sensors and fill lights on both sides of the protective shell to provide real-time feedback on relevant information in the tunnel to prevent unexpected situations. At the same time, the protective shell is used as a steering gear support platform of the working platform to place the steering gear and achieve a rotating degree of freedom for the rotating platform.

1.4 Laser De-Icing Patrol Unit Overall Program Design

A two-degree-of-freedom rotating platform is used to connect the laser and camera to ensure that the laser de-icing inspection device effectively covers the entire tunnel roof area. This platform can be flexibly adjusted to various horizontal and tilt angles. The structure of the connection unit is shown in Fig. 4.

The L-type horizontal rotating abutment is securely fastened to the horizontal plane of the protective shell using the rudder plate and the horizontal rotating platform, allowing the working platform to rotate freely in the horizontal direction. The vertical rotating platform is fixed in the vertical plane of the L-type horizontal rotating platform, connected with the C-type vertical rotating platform by the rudder plate to realize the free rotation of the vertical direction of the working platform. Both the horizontal rotating servo and vertical rotating servo have a rotation angle of 180°. The laser is positioned within the square slot hole, while the binocular camera is firmly mounted on the vision board.

2 ANALYSIS OF THE MECHANISM OF LASER ACTION ON ICE

2.1 Laser Power Distribution

Lasers are a type of Gaussian beam [47]. Due to the highly focused energy of the laser beam, its extremely high power density enables lasers to deliver a large amount of energy in a very short period, thereby achieving efficient heating [48]. Their power distribution is generally described using a Gaussian function. At the centre of its cross-section, the laser intensity reaches its maximum, and the farther away from the centre, the weaker the light intensity becomes, decreasing exponentially with the square of the distance. Considering that ice is a solid form of water, the thickness, density, structure, and other characteristics of the ice layer can affect the transmission and absorption efficiency of laser power, thus influencing the effectiveness of de-icing [49], the thermal effect of the laser on the icicle can be visualized as occurring within an infinitely thin region. In this context, the laser can be treated as a surface heat source, as illustrated in Eq. (1), since the

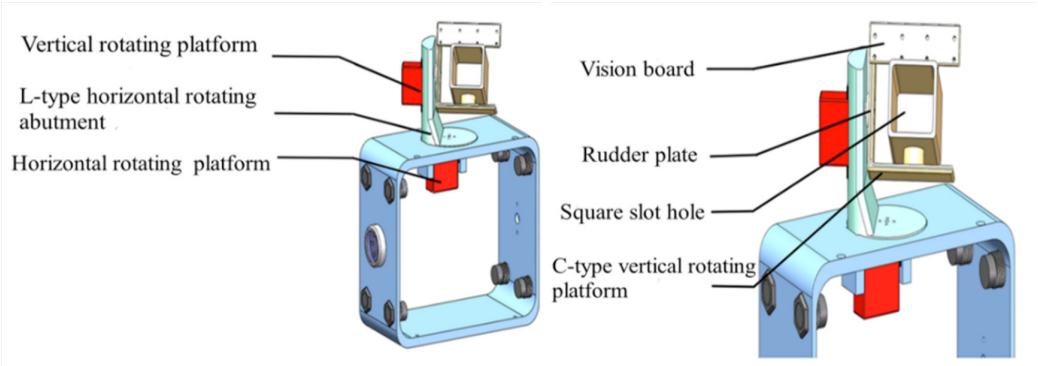

Fig. 4. *Structure of the connection unit*

absorption of the laser primarily takes place on the surface of the ice:

$$I = \frac{2AP_1}{\pi R^2} e^{\frac{-2r^2}{R^2}}, \quad (1)$$

where I denotes the laser power density [W/m^2]; P_1 denotes the laser power [W]; A denotes the laser absorption rate [-]; r denotes the distance from the centre of the laser spot [m]; R denotes the radius of the laser spot [mm].

2.2 Temperature Distribution of Laser Heating

In the process of studying the internal temperature distribution of the material after laser irradiation, we need to make the following assumptions about the material and its thermophysical properties:

It is assumed that the size of the material under study is infinite and that the solid remains solid during heating by the laser;

There is no effect of the temperature on the thermal properties of the material;

The heat loss generated by the action at the surface is neglected.

Then, the variation of the solid surface temperature field under the action of a stationary laser beam can be expressed as Eq. (2):

$$T - T_0 = \\ = \frac{AP_1}{k\pi^{3/2}R} \int_0^{\sqrt{\frac{A\alpha t}{R^2}}} \frac{1}{1+u^2} \cdot \exp\left[-\frac{z^2}{R^2u^2} - \frac{x^2+y^2}{R\left(1+u^2\right)} \right] du, \quad (2)$$

where T and T_0 denote the temperatures after and before heating, respectively, [°C]; t denotes the heating time [s]; α denotes the thermal diffusion coefficient [m^2/s]; k denotes the thermal conductivity of the material in [W/(m·°C)]; where $u = \sqrt{t - t'}$ and $t–t'$ denotes the time increment [-]; x, y, and z are the coordinates of the laser irradiation point.

From Eq. (2), the temperature at the centre of the laser spot ($x=y=z=0$) with the time change rule can be expressed as Eq. (3):

$$T = T_0 + \frac{AP_1}{k\pi^{3/2}R} \arctan \sqrt{\frac{A\alpha t}{R^2}}. \quad (3)$$

Under laser irradiation, the surface of the material is rapidly heated as the laser beam makes contact. However, the surrounding area, centred on the focal point, does not have enough time to reach a stable temperature state. Consequently, the heat absorbed on the surface continues to be conducted towards the inner layers of the material, facilitating thermal fusion within the material's core.

2.3 Calculation of De-Icing Energy Consumption Based on the Law of Conservation of Energy

The law of conservation of energy, also known as the first law of thermodynamics, clearly illustrates the principle of energy transfer. In other words, energy cannot be created or destroyed; it can only be transferred from one object to another or converted from one form to another [50]. Throughout this conversion or transfer process, the total amount of energy in a closed system remains constant. This is because any heat transfer process must comply with the law [51].

According to the law of the conservation of energy, the relationship between the energy E consumed by the laser and the time of laser irradiation t is expressed as Eq (4).

$$E = P \cdot t, \quad (4))$$

where P represents the laser power [W]. Using this formula, we can calculate the total laser energy required to remove the ice body, thus enabling the calculation of de-icing energy consumption, that is, the laser energy needed to remove a unit volume of ice (J/mm^3). This, in turn, forms a theoretical foundation for further analysis of the energy consumption involved in laser de-icing.

3 SIMULATION ANALYSIS OF LASER DE-ICING PROCESS

We used the Fluent module in ANSYS software to simulate the de-icing process under laser irradiation, analysed the energy consumption changes of laser de-icing, and simulated the energy consumption changes under three variables, laying the foundation for subsequent experiments.

Due to the complex geometry of icicles, unstructured meshes can more easily adapt to the geometric characteristics of the model and provide greater flexibility while reducing the overall element count without sacrificing accuracy, effectively utilizing computing resources. We conducted a grid independence study. By gradually refining the grid, we compared the simulation results under different grid densities. Through the grid independence study, we can ensure the validity of the simulation results.

Before conducting the simulation analysis, it is essential to simplify the design of the icicle model. In practical de-icing scenarios, the icicle to be treated

often has a certain length, and its central vertical cross-section closely resembles an isosceles triangle, as depicted in Fig. 5.

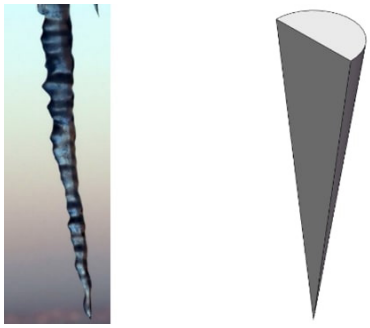

Fig. 5. *Schematic vertical cross-section of icicle centre*

During the de-icing process, the laser is injected from below diagonally and acts close to the root of the icicle. As a result, in the simulation, it is unnecessary to model the entire icicle; only a certain length of the icicle close to its base needs to be considered. The icicle's cross-section at this length is theoretically trapezoidal. However, due to its nearly 90° bottom angle, for simplicity in calculations, the simulation model assumes an equal-length cylinder with a diameter of 60 mm and a height of 100 mm. The laser incidence point is set at the lower-left corner with an angle of 45°, as depicted in Fig. 6.

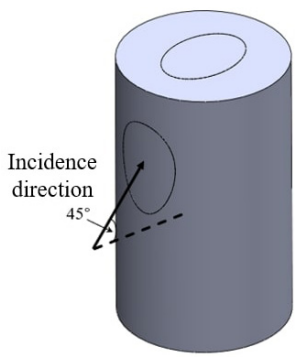

Fig. 6. *Diagram of the icicle model*

In ANSYS software, the system can automatically divide the grid according to the physical size of the model, but the accuracy of the grid after automatic division is low, and the accuracy of the simulation data is poor. To ensure the accuracy of simulation data, it is necessary to manually divide the grid, especially in the place of laser irradiation, which is the main part of heat transfer, and the grid division needs to be more precise and detailed. The meshing results are illustrated in Fig. 7.

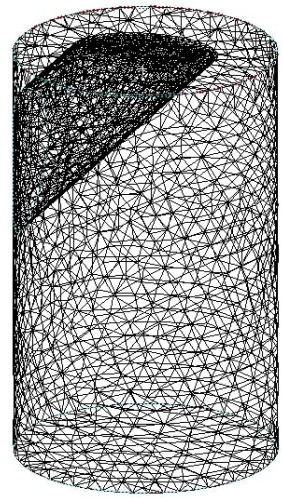

Fig. 7. *Grid division results*

During the actual de-icing process, when the laser heats the icicle, a phase transition from solid water to liquid water occurs. Dealing with this transition in simulations can be very complex, as it involves numerous parameter changes, which can be challenging for accurate calculations. To circumvent these complexities and avoid the phase transition in the simulation process, a technique known as the “kill the grid” method is employed, which involves discarding the portion of the model where the heat causes melting and transforms ice into water. By doing this, the simulation proceeds with the laser directly irradiating the next layer of ice, and so on, without considering the phase transition. This approach not only simplifies the computational aspect but also offers more intuitive observations of the laser de-icing simulation results.

3.1 Simulation Results Under Temperature Variation

According to the delineated grid model, its de-icing under different ambient temperatures is analysed. The distance between the laser and the icicle is set to be 2 m, the wind speed of the outside environment is selected to be 2m/s, and the initial temperatures of the icicle are -5 °C, -10 °C, -15 °C, and -20 °C. The icicle was irradiated with a laser for 200 seconds at four different temperatures, and its internal temperature distribution is shown in Fig. 8.

In Figs. 8 to 13, "MN" and "MX" represent the minimum value (Minimum) and the maximum value (Maximum), respectively. These indicators are used to identify the range and extreme values of the temperature distribution within the simulation area.

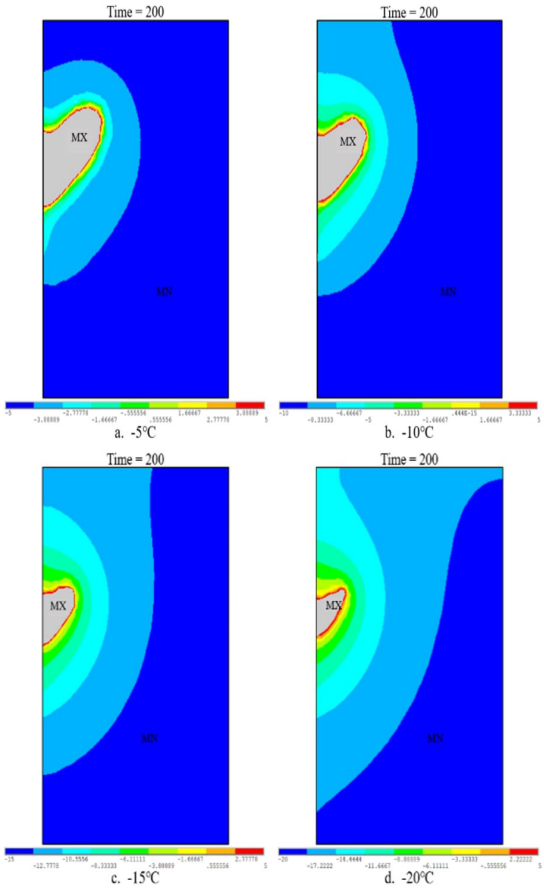

Fig. 8. *Temperature distribution inside the icicle at four temperatures with laser irradiation for 200 s*

In the Fig. 8, the blue area represents the non-melted portion of the icicle. The closer the area is to the warm colour, the higher the heating temperature. The grey area represents the cavities formed when the ice melts into the water at temperatures above 5 °C. The depth of the grey area reflects the extent of laser penetration into the icicle, with deeper grey areas indicating more extensive ice melting and a more effective de-icing outcome.

As can be seen from Fig. 8, within the same duration of laser exposure, the variation in melt-through depth formed by laser irradiation under four initial temperatures is significant. Measured using software, the depths of melt-through are approximately 19.1 mm, 14.6 mm, 10.9 mm, and 8.6 mm, respectively. This indicates that the closer the initial temperature of the icicle is to 0 °C, the deeper the laser penetrates the model and the better the de-icing effect.

Using lasers, the icicles were heated at four outside temperatures until they were completely melted through, as shown in Fig. 9. The time taken to achieve complete melting was recorded to calculate the de-icing energy consumption, and the results are presented in Table 1.

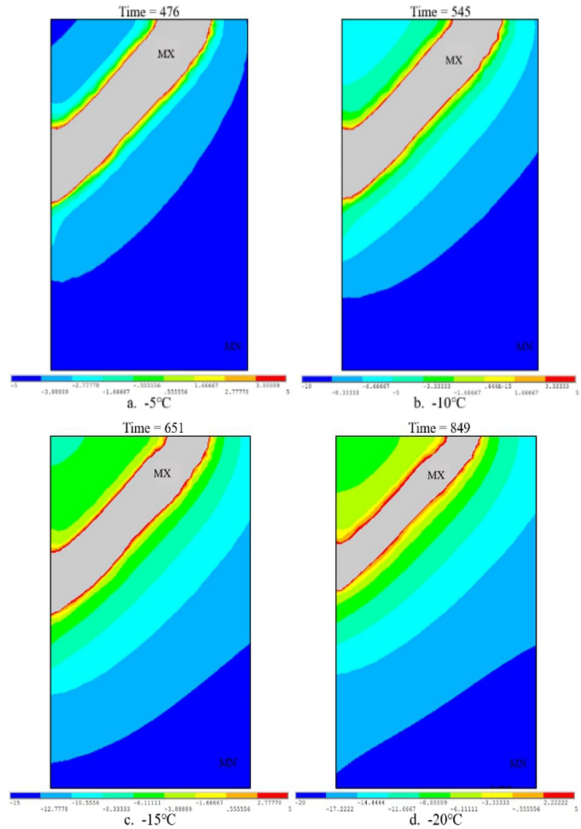

Fig. 9. *Temperature distribution inside the icicle at four temperatures for complete laser melting through the icicle*

Table 1. *Effect of different temperatures on de-icing energy consumption*

De-icing volume [cm³]	13.139			
Temperature [°C]	–5	–10	–15	–20
Time required [s]	476	545	651	849
De-icing energy consumption [J/mm³]	1.45	1.66	1.98	2.58

The de-icing volume in Table 1 can be measured in SolidWorks. As can be seen from Table 1, in the removal of a fixed amount of icicle, the lower the external temperature, the longer the laser irradiation time required; on the contrary, the higher the external temperature, the shorter the laser irradiation time required, the less heat consumption, that is, the lower the de-icing energy consumption.

In practical applications, due to the gravity of the icicle itself, in the process of melting through a certain point of the icicle, with the diffusion of laser energy in the icicle, the adhesion between the icicle

and the tunnel wall is also reduced, so that the icicle is separated under the action of its own gravity, so as to achieve the effect of de-icing. If the icicle does not break free under its own gravity, it can be de-iced a second time at a nearby point until the icicle falls off. In this study, only one icicle melting penetration test was carried out during the simulation and subsequent experiments.

3.2 Simulation Results Under Distance Variation

During the simulation process, directly reflecting the distance between the icicle and the light source is not feasible, and the laser in the air is scattering, resulting in larger spot sizes at farther distances. Therefore, the change in distance can be reflected by the size of the diameter of the spot. For the simulation, the initial temperature of the icicle is set to -10 °C, the ambient wind speed is 2 m/s, and the distance between the experimental laser and the icicle is pre-set to be 1.5 m, 2 m, 2.5 m, and 3 m, with corresponding spot sizes of 12 mm, 14 mm, 16 mm, and 18 mm, respectively. Heating simulations are conducted for the icicle with these four different spot radii, and the internal temperature distributions when heated up to 200 seconds are shown in Fig. 10.

As observed from Fig. 10, as the distance increases, the melting hole becomes larger. Simultaneously, the dispersion of laser energy due to the larger spot size leads to energy being distributed over a broader area on the icicle's surface. Consequently, the depth of the melting hole becomes shallower. The measured depths of the melt-through are 16.1 mm, 14.6 mm, 12.3 mm, and 10.2 mm, corresponding to the distances of 1.5 m, 2 m, 2.5 m, and 3 m. This means that the closer the distance between the icicle and the laser, the deeper the melting hole's depth within the icicle.

Lasers are used to heat the icicles at four different distances until they are completely melted through, as shown in Fig. 11.

Furthermore, the time taken for the laser to completely melt through the icicle was recorded to

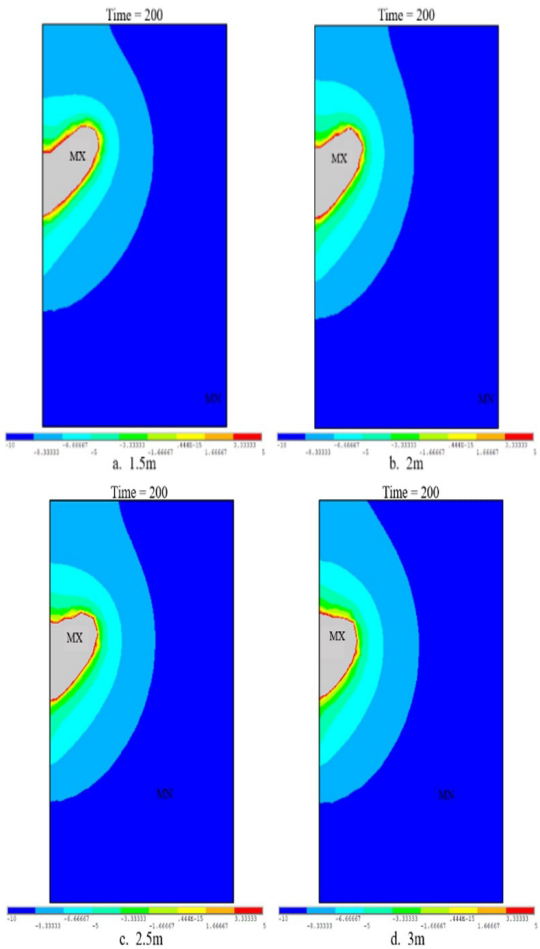

Fig. 10. *Temperature distribution inside the icicle during 200 s of laser irradiation at four distances*

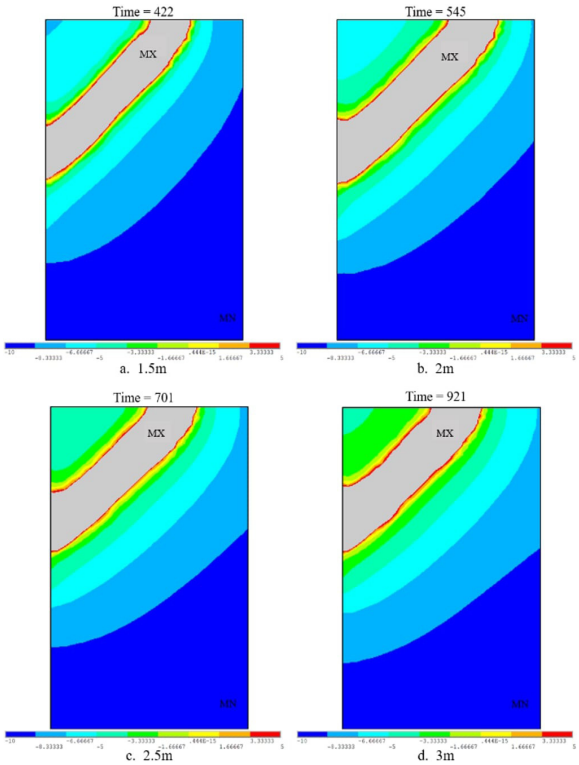

Fig. 11. *Temperature distribution of the laser completely melting through the icicle at four distances*

calculate the de-icing energy consumption. The results are shown in Table 2.

Table 2. *Effect of different distances on de-icing energy consumption*

De-icing volume [cm³]	13.139			
Distance [m]	1.5	2	2.5	3
Time required [s]	422	545	701	921
De-icing energy consumption [J/mm³]	1.58	1.66	1.77	1.96

It can be observed that under the condition of melting through the same volume of an icicle, the required laser irradiation time increases with the distance. That is, as the distance between the laser emitter and the icicle increases, the required irradiation time becomes longer, resulting in higher de-icing energy consumption. Conversely, as the distance decreases, the irradiation time becomes shorter, leading to lower de-icing energy consumption.

3.3 Simulation Results Under Wind Speed Variation

In this study, the initial temperature of the icicle is set to –10 °C, the distance between the laser and the icicle is fixed at 2 m, and the wind speeds are set to 2 m/s, 3 m/s, 4 m/s, and 5 m/s. Each laser irradiates the icicle for 200 seconds under these four different wind speeds, and the distribution of its internal temperature is illustrated in Fig. 12.

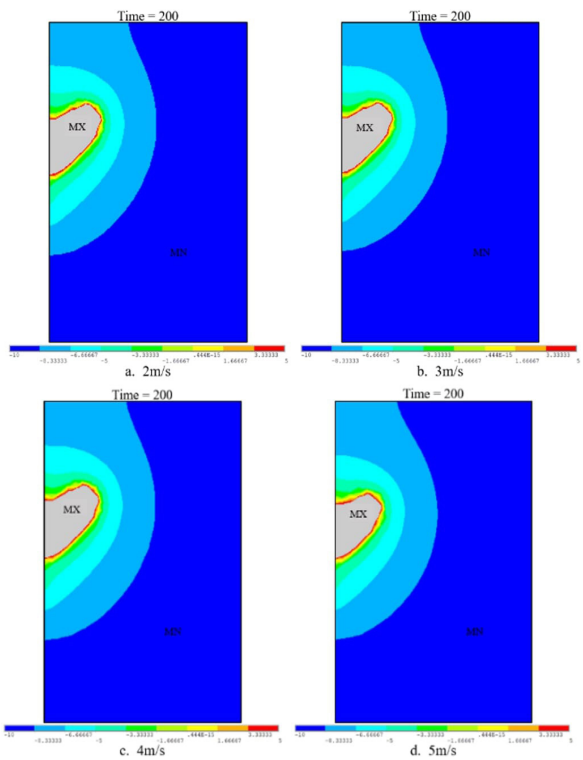

Fig. 12. *Temperature distribution inside the icicle during 200 s of laser irradiation under four wind speeds*

As can be seen from Fig. 12, in the same laser irradiation time, the four different wind speeds result in varying depths of melting through the ice. Higher wind speeds lead to shallower depths of melting through, with measurements corresponding to approximately 14.6 mm, 14.2 mm, 13.8 mm, and 13.3 mm, respectively. In other words, lower wind speeds yield a more effective de-icing outcome.

Continue heating the icicles at the four wind speeds until they are completely melted through, as illustrated in Fig. 13. Then, statistical analysis are conducted on the time taken for the laser to fully melt through the icicle in order to calculate the de-icing energy consumption. The results are presented in Table 3.

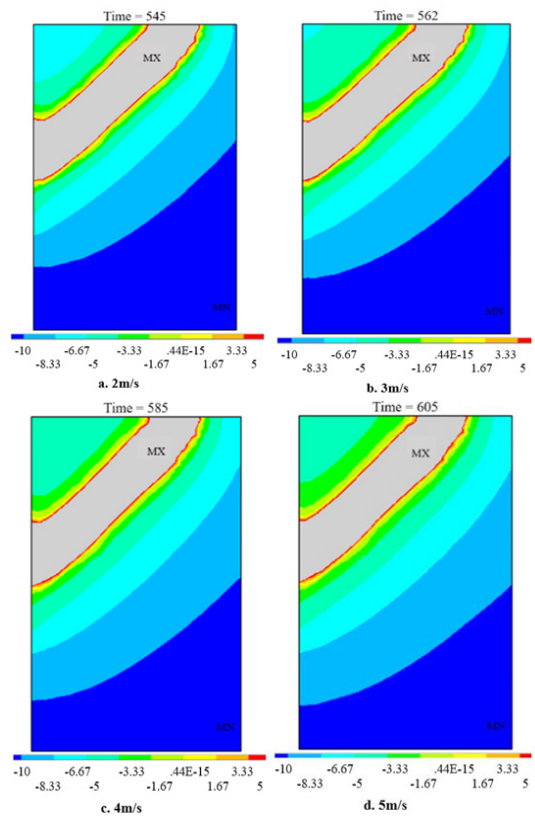

Fig. 13. *Temperature distribution of laser completely melting through the icicle at four wind speeds*

As observed from Table 3, under the same conditions of melting through the same volume of icicles, the laser irradiation time increases with an increase in wind speed. In other words, higher external wind speeds result in longer laser irradiation times and

higher energy consumption. Conversely, lower wind speeds lead to shorter irradiation times and reduced energy consumption for clearing the same unit volume of ice, resulting in lower de-icing energy consumption.

Table 3. *Effect of different wind speeds on de-icing energy consumption*

De-icing volume [cm³]	13.139			
Wind speed [m/s]	2	3	4	5
Time required [s]	545	562	585	605
De-icing energy consumption [J/mm³]	1.66	1.71	1.78	1.84

4 TUNNEL LASER DE-ICING PATROL DEVICE EXPERIMENT AND ENERGY CONSUMPTION ANALYSIS

4.1 Laser De-Icing Patrol Device Test Prototype Construction

To further investigate the effectiveness of the laser de-icing inspection device and validate the accuracy of the simulation calculations, a test prototype is prepared based on the established device model, as illustrated in Fig. 14. The device comprises three main components: the rail module, the base platform, and the working platform. Electrical appliances are connected to the battery through wires, with most of the wires placed within the base platform. The wires are wrapped in a protective shell to ensure the device's safety, avoiding damage and preventing issues such as wire rupture and electrical leakage.

Fig. 14. *Test prototype of laser de-icing inspection device*

A detailed analysis of laser de-icing energy consumption was carried out in the laboratory using the prepared test prototype, with the findings being compared to simulation data.

4.2 Experimental Testing of Laser De-Icing

In the experimental test, the initial step involves the laser melting through the icicle. In practical de-icing operations, if the first melt-through fails to make the icicle at the top of the tunnel fall off under its own gravity, the laser can be directed to other locations on the icicle for a second melt-through. This process allows the laser energy to continue diffusing inside the icicle until the icicle eventually detaches.

4.2.1 Experimental Results Under Temperature Variation

The distance between the laser and the icicle is set to be 2 m, the wind speed of the outside environment is selected to be 2 m/s, and the initial temperatures of the icicle are –5 °C, –10 °C, –15 °C, and –20 °C, as depicted in Fig. 15.

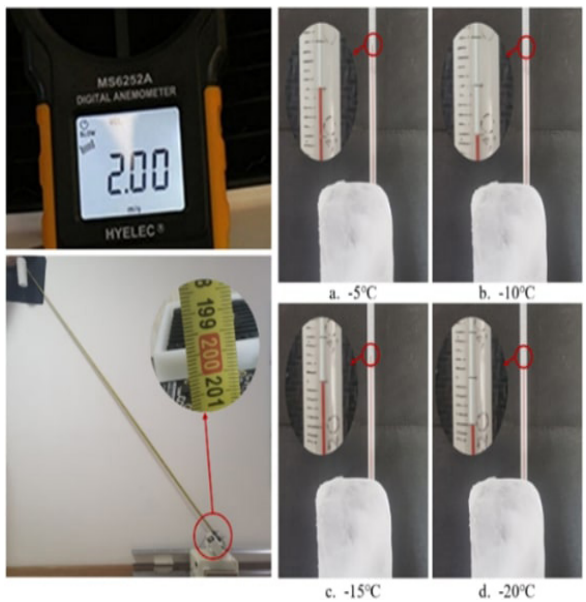

Fig. 15. *Setting of environmental conditions under temperature change*

When the icicle is heated at different initial temperatures for 200 s, stop heating, and the melt-through depth is measured. The results, depicted in Fig. 16, show melt-through depths of 17.77 mm, 13.43 mm, 10.58 mm, and 7.83 mm, respectively, for initial temperatures of –5 °C, –10 °C, –15 °C, and –20 °C. Comparing these measurements with the simulation results, it is evident that the depth of laser melt-through for each temperature is slightly smaller than that of the simulation results. However, the trend of melt-through depths for the four temperatures remains consistent. Subsequently, the laser heating

is resumed at the same angle and distance from the previous melting site, and the timing is restarted until the icicle is completely melted through. The timing is then stopped, and the previous 200 s are added to calculate the total laser heating time. The results of the melt-through icicle are shown in Fig. 17.

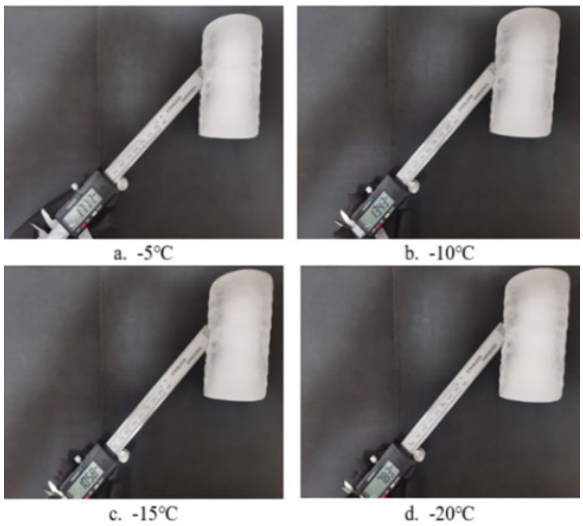

Fig. 16. *Experimental results of laser heating of icicle for 200 s at four temperatures*

Fig. 17. *Laser melting through icicles*

As the laser incidence angle cannot be guaranteed to be the same during the experimental process, even a slight difference can lead to variations in the de-icing volume. A weighing method is used to calculate the amount of ice removed accurately. By measuring the mass before and after laser penetration and calculating the difference between the two, the volume of ice removed is determined. The de-icing energy consumption is then calculated, and the results are shown in Table 4.

The experimental environment is configured based on the conditions of the simulation setup. The initial temperature of the icicle is set to –10 °C, while the ambient wind speed is maintained at 2 m/s. The distances between the laser and the icicle are set at 1.5 m, 2 m, 2.5 m, and 3 m, as illustrated in Fig. 18.

Table 4. *Experimental results of de-icing energy consumption at four temperatures*

De-icing volume [cm³]	12.2	13.6	13.3	12.8
Temperature [°C]	–5	–10	–15	–20
Time required [s]	467	592	755	906
De-icing energy consumption [J/mm³]	1.53	1.74	2.27	2.83

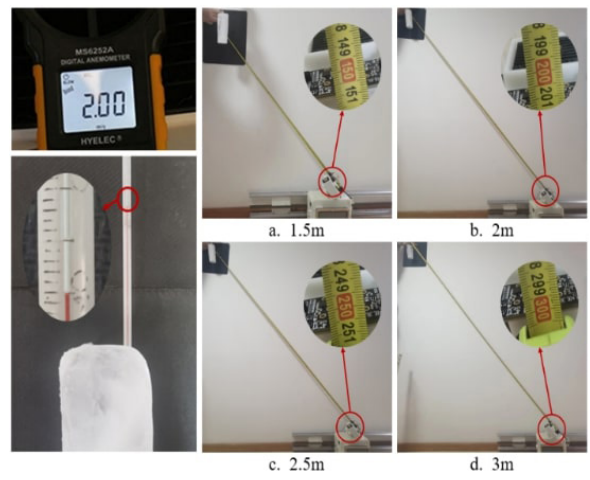

Fig. 18. *Setting of environmental conditions under distance variation*

4.2.2 Experimental Results Under Distance Variation

The laser was directed into the icicle from the lower left at a 45° angle. However, due to varying distances, the size of the laser spot on the icicle differed, as depicted in Fig. 19. To evaluate the depth of melt-through at 200 seconds of laser irradiation, measurements were taken at four different distances. The results are illustrated in Fig. 20. Continued heating and melting through the icicle after measurement. Due to the different sizes of the light spots, the size of the fused holes also changed. The result of the fused hole is shown in Fig. 21.

Fig. 20 shows that the depths of melt-through were 14.52 mm, 13.43 mm, 11.51 mm, and 8.93 mm. The corresponding melt-through durations are recorded and summarized in Table 5.

Table 5. *Experimental results of de-icing energy consumption at four distances*

De-icing volume [cm³]	11.7	13.6	14.9	20.1
Distance [m]	1.5	2	2.5	3
Time required [s]	538	592	630	763
De-icing energy consumption [J/mm³]	1.84	1.74	1.69	1.52

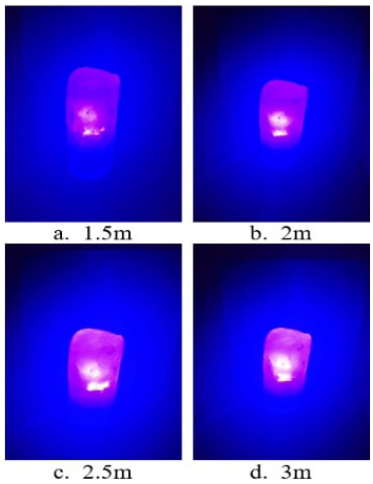

Fig. 19. *Spots on the icicle presented by the laser at different distances*

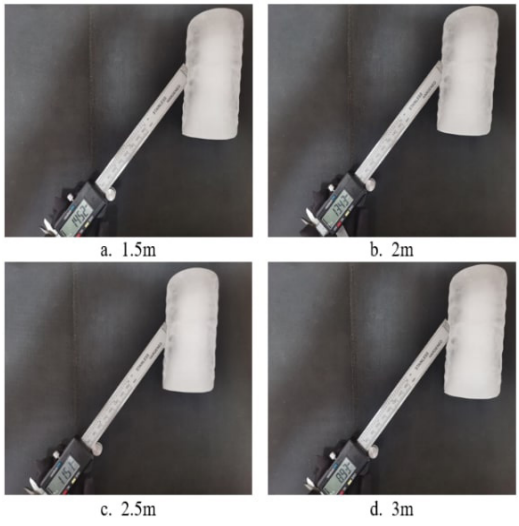

Fig. 20. *Experimental results of laser heating of icicles for 200 s at four distances*

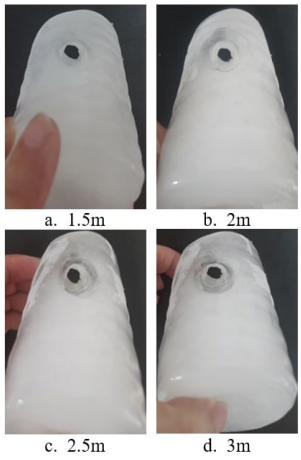

Fig. 21. *Results of icicle melt-through at different distances*

4.2.3 Experimental Results Under Wind Speed Variation

The experimental environment is designed to match the conditions of the simulation setup. The initial temperature of the icicle is set to –10 °C, and the distance between the laser and the icicle is fixed at 2 m. Additionally, the wind speeds tested are 2 m/s, 3 m/s, 4 m/s, and 5 m/s, as illustrated in Fig. 22.

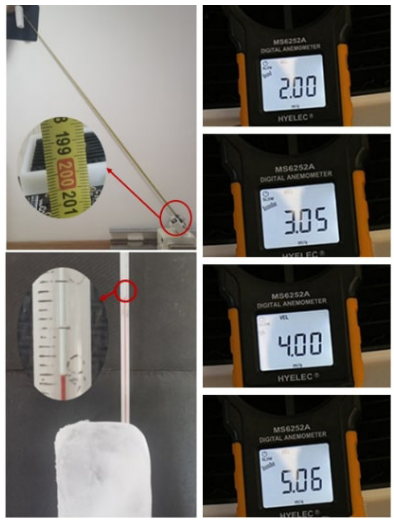

Fig. 22. *Setting of environmental conditions under wind speed variation*

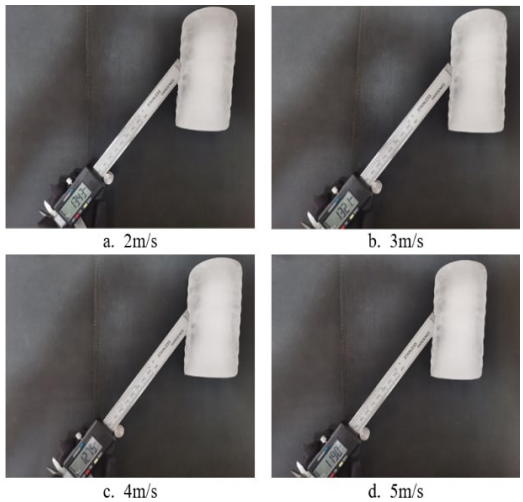

Fig. 23. *Experimental results of laser-heated icicles for 200 s at four wind speeds*

The laser is consistently injected into the icicle from the lower left at a 45° angle, and its spot size remains constant irrespective of the distance. Consequently, the laser irradiation effect on the icicle is similar to that under the initial temperature change. To measure the melting depth, the laser was irradiated

at the icicle for 200 s at various wind speeds. The results of these measurements are presented in Fig. 23.

Table 6. *Experimental results of de-icing energy consumption under four wind speeds*

De-icing volume [cm³]	13.6	13.1	13.2	13.7
Wind speed [m/s]	2	3	4	5
Time required [s]	592	577	598	648
De-icing energy consumption [J/mm³]	1.74	1.76	1.81	1.89

The depths of melt-through were 13.43 mm, 13.21 mm, 12.75 mm, and 11.90 mm. Subsequently, we proceeded to further melt through the icicle using the aforementioned method of heating. The melt-through effect was found to be similar to that observed during the initial temperature change of the icicle. The duration of the melt-through was recorded, and the results are presented in Table 6.

5 COMPARISON ANALYSIS OF EXPERIMENTAL AND SIMULATION RESULTS

The experimental data were meticulously organized and analysed in conjunction with the simulation results. The melt-through depth of the laser at 200 s and the corresponding de-icing energy consumption data for the three variables were represented as line graphs, illustrated in Figs. 24 to 26, respectively.

In this experiment, the wavelength is not within the test range, and all wavelengths are the same. The CO_2 laser we use operates at a wavelength of 10.6 μm. The device's de-icing energy consumption was analysed by changing three variables: the icicles' initial temperature, the distance between the laser and the icicles, and the ambient wind speed.

When considering a single variable, if the initial temperature of the icicle decreases at a constant distance and wind speed, the depth of the laser's melting penetration in the same amount of time

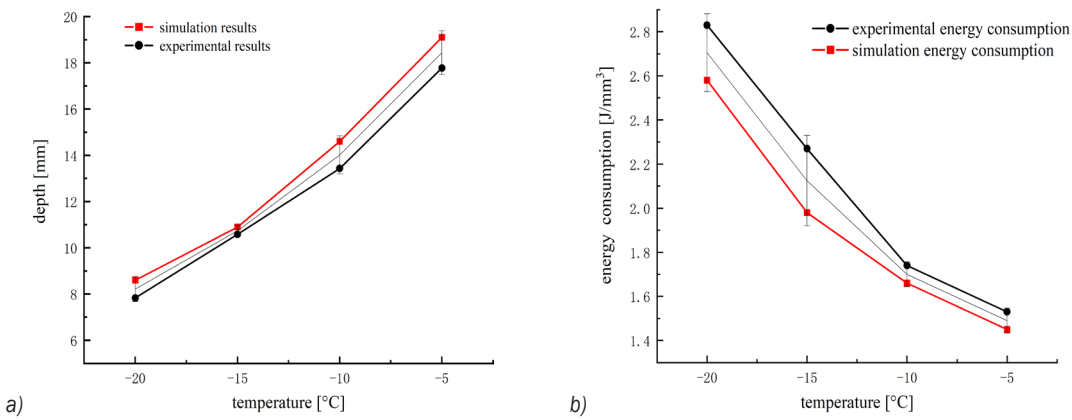

Fig. 24. *Effect of temperature change on de-icing energy consumption; a) comparison of ice melt depth in 200 s, and b) comparison of de-icing energy consumption*

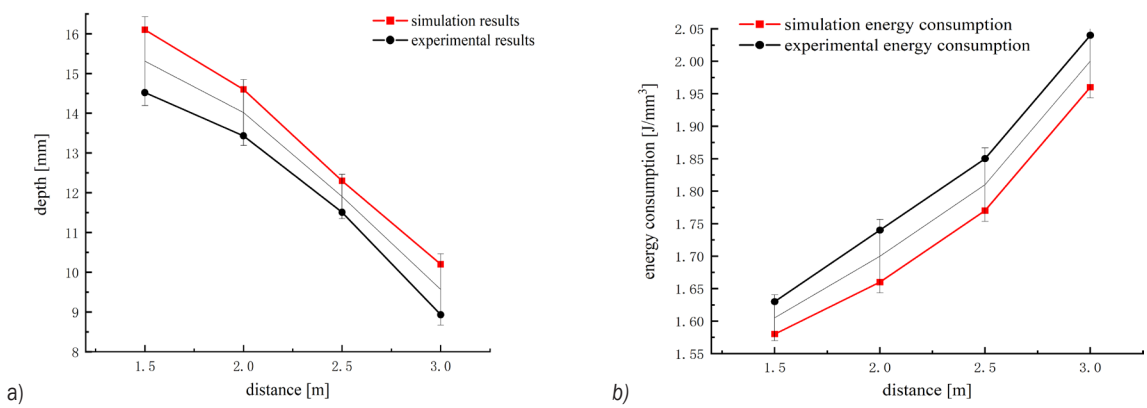

Fig. 25. *Effect of distance variation on de-icing energy consumption; a) comparison of ice melt depth in 200 seconds* and b) Comparison of de-icing energy consumption

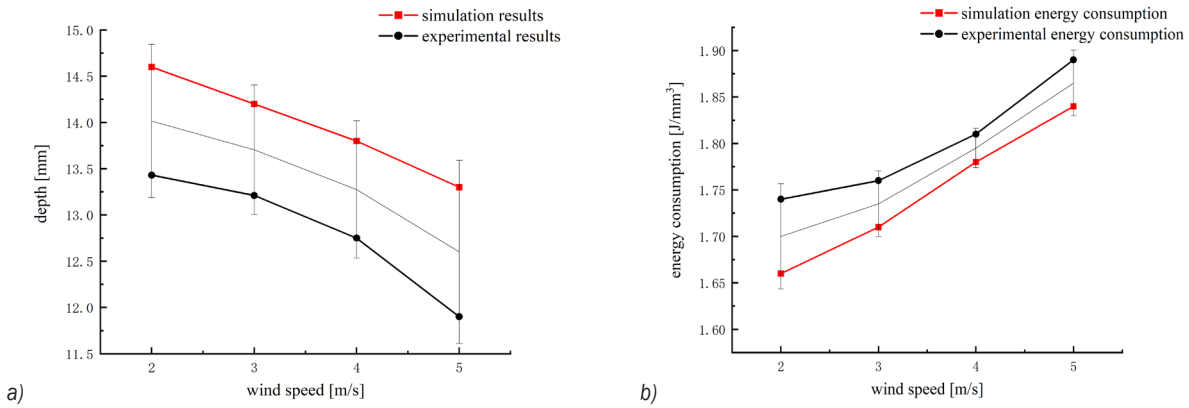

Fig. 26. *Effect of wind speed variation on de-icing energy consumption; a) comparison of ice melt depth in 200 s, and b) comparison of de-icing energy consumption*

becomes shallower, and the energy consumption for de-icing increases. This is because a lower initial temperature of the icicle demands more energy to reach the melting point after heating, resulting in longer laser action time per unit volume of ice.

Under the condition of constant initial temperature and wind speed, when the distance between the light source point and the icicle is continuously lengthening, the depth of laser melting penetration in the same period will also become shallower and shallower, but its overall de-icing energy consumption is decreasing. This is due to changes in the distance caused by changes in the radius of the spot irradiated on the icicle; the farther the distance, the larger the spot, the larger the heated area on the icicle, and the energy is more dispersed, to remove the volume of ice increased at the same time reduce the speed of melting ice. However, from the point of view of the decreasing energy consumption of de-icing, the rate of increase of de-icing volume is greater than the rate of increase of heating duration, so the energy required to remove the unit volume of ice decreases with the increase in distance, resulting in a more efficient de-icing process.

Under the condition of constant initial temperature and distance, when the ambient wind speed increases, the melting depth of the laser will keep getting shallower at the same time, and its overall de-icing energy consumption continues to increase. This is because, as wind speed increases, the effect of airborne particles on the laser intensifies, leading to greater energy loss. In the experimental setup, compared to simulations, the wind speed causes a continuous impact of new particles on the laser, resulting in greater energy loss in the air. Therefore, the energy required to remove a unit volume of ice increases with the increase in wind speed.

Although there is a slight difference between the experimental and simulation results, the overall trend remains consistent. This further validates the accuracy of the simulation and confirms its reliability in predicting real-world outcomes. Analysing the comparison results of the three variables in conjunction with practical scenarios, it becomes evident that the temperature range exhibits more significant fluctuations, making it a key factor influencing the laser's energy consumption for de-icing. Wind speed, except in special cases, generally remains within a fixed range. Additionally, the distance between the laser and the icicle can be controlled within a certain range according to the height of the tunnel.

7 CONCLUSIONS

Aiming at the problem that icicle removal is not convenient, a laser de-icing device is designed, and its energy consumption is analysed as follows:

(1) A modularized design approach is utilized to develop a tunnel laser de-icing inspection device, comprising three major modules: the track module, the base platform, and the working module.

(2) The laser de-icing process was simulated and analysed using ANSYS simulation software. The melting depth of laser irradiation for 200 s and the time taken for complete melting were simulated when the initial temperature of the icicle was –5 °C, –10 °C, –15 °C, –20 °C, the distance between the laser and the icicle was 1.5 m, 2 m, 2.5 m, 3 m, and the wind speed was 2 m/s, 3 m/s, 4 m/s, and 5 m/s, respectively, under the three variables of laser irradiation. It is concluded that the higher the initial temperature, the closer the distance,

and the lower the wind speed, the lower the energy consumption of de-icing.

(3) A prototype tunnel laser de-icing inspection device was assembled, and its de-icing energy consumption was experimentally analysed. In the same laboratory environment as the simulation setting, the laser irradiation depth at 200 s and the time taken for complete melting were measured. A comparison with the simulation results reveals that the experimental melting depth at 200 s is slightly smaller, and the time required for complete melting is slightly longer. Consequently, the energy consumption for laser de-icing in the experiment is slightly higher than in the simulation. The comprehensive analysis shows that the trend of the experimental results and the simulation results are consistent, which also makes the experimental results and the simulation results mutually verified.

8 ACKNOWLEDGEMENTS

The work described in this paper has been supported by the Fundamental Research Program of China's Shanxi Province (20210302123038), the Special project of Scientific and Technological Cooperation and Exchange of China's Shanxi Province (202104041101001), and the North University of China Science and Technology Project (20231915). The authors would like to express their heartfelt gratitude for the support of this study.

9 REFERENCES

[1] Yan, J., Wei, Y.Q., He, C., Zhou, Z.H., Gou, H. (2020). Sichuan-Tibet Highway hot-freeze link technology and its application in snow melting and deicing at tunnel entrance. *Modern Tunnelling Technology*, vol. 57, no. 5, p. 1-9, **DOI:10.13807/j.cnki.mtt.2020.05.001**. (in Chinese)

[2] Yu, T., Qiao, L., Liu, X. (2021). Cable deicing device based on ice melting and mechanical ice breaking. Journal of Physics: Conference Series, vol. 1865, no. 03, **DOI:10.1088/1742-6596/1865/3/032074**.

[3] Tamer, O., Walter, F., Sinapius, M., Böl, M. (2022). A computational geometric parameter optimization of the thermomechanical deicing concept. Actuators, vol. 11, no. 08, DOI:10.3390/act11080223.

[4] Wang, Y., An, Z.L., Ma, W.B., Zheng, Z.F., Guo, X.X. (2022). State-of-art and development trend of tunnel inspection technology in China, Japan, and South Korea. *Tunnel Construction*, vol. 42, no. 07, p. 1135-1145, **DOI:10.3973/j.issn.2096-4498.2022.07.002**. (in Chinese)

[5] Zhou, W., Liao, S., Men, Y. (2021). A fluid-solid coupled modeling on water seepage through gasketed joint of segmented tunnels. *Tunnelling and Underground Space Technology*, vol. 114, **DOI:10.1016/j.tust.2021.104008**.

[6] He, Q., Lv, X.-f., Zhao, X.-t. (2014). Overhead transmission lines deicing under different incentive displacement. *Journal of Applied Mathematics*, vol. 2014, p. 1-8, **DOI:10.1155/2014/872198**.

[7] He, H., Huang, W., Guo, Z. (2023). Superhydrophobic and photothermal sic/tin durable composite coatings for passive anti-icing/active de-icing and de-frosting. *Materials Today Physics*, vol. 30, **DOI:10.1016/j.mtphys.2022.100927**.

[8] Guo, C., Liao, R., Yuan, Y., Zuo, Z., Zhuang, A. (2015). Glaze icing on superhydrophobic coating prepared by nanoparticles filling combined with etching method for insulators. *Journal of Nanomaterials*, vol. 2015, p. 1-7, **DOI:10.1155/2015/404071**.

[9] Song, L., Yang, C., Zhang, S., Wang, Y., Zou, R., Cheng, E., Lee, A., Deng, Q. (2022). Multifunctional photothermal phase-change superhydrophobic film with excellent light-thermal conversion and thermal-energy storage capability for anti-icing/de-icing applications. *Langmuir*, vol. 38, no. 49, p. 15245-15252, **DOI:10.1021/acs.langmuir.2c02329**.

[10] Jiang, L., Han, M., Sun, J., Gong, M., Lin, Y., Xiao,T., Xiang, P., Chen, W., Tan, X. (2023). Strong mechanical and durable superhydrophobic photothermal mwcnts/sio2/pdms/pvdf composite coating foranti-icing and de-icing. *Progress in Organic Coatings*, vol. 174, **DOI:10.1016/j.porgcoat.2022.107282**.

[11] Gao, L., Liu, Y., Ma, L., Hu, H. (2019). A hybrid strategy combining minimized leading-edge electric-heating and superhydro-/ice-phobic surface coating for wind turbine icing mitigation. *Renewable Energy*, vol. 140. p. 943-956, **DOI:10.1016/j.renene.2019.03.112**.

[12] Jiang, M., Zhao, H.D., Ma, X.Q. (2020). Overview of icing, anti-icing and de-icing technologies for high-voltage transmission lines. *Electric Safety Technology*, vol. 22, no. 4, p. 26-32, **DOI:10.3969/j.issn.1008-6226.2020.04.008**. (in Chinese)

[13] Tang, B.H., Wang, Q., Han, X.C., Zhou, H., Yan, X.J., Yu, Y., Han, D.D. (2022). Fabrication of anti-icing/de-icing surfaces by femtosecond laser. *Frontiers in Chemistry*, vol. 10, p. 1073473, **DOI:10.3389/fchem.2022.1073473**.

[14] Wei, X., Zhong, Y., Feng, Y., Wei, J., Wang, J. (2022). A slippery liquid-infused network-like surface with anti/de-icing properties constructed based on the phosphating reaction. Langmuir, vol. 38, no. 46, p. 14118-14128, **DOI:10.1021/acs.langmuir.2c02075**.

[15] Mo, Q.Y., Wang, G.Q., Guo, R.B., Li, L., Liu, Y.Y. (2022). Icing status of wind turbine blades and anti-icing and de-icing measures. *Science Technology and Engineering*, vol. 22, no. 21, p. 9017-9024, **DOI:10.3969/j.issn.1671-1815.2022.21.002**. (in Chinese)

[16] Zhu, C.X., Zhu, C.L., Zhao, W.W., Tao, M.J. (2017). Experimental study on the shear adhesion strength between the ice and substrate in icing wind tunnel. *Journal of Mechanics*, vol. 34, no. 2, p. 209-216, **DOI:10.1017/jmech.2017.83**.

[17] Hou, Y., Wang, M., Choy, K.-L. (2022). Scalable high-efficiency multilayered anti-icing/de-icing coating: Superhydrophobic upper layer boosts the performance of the electrothermal system. *Progress in Organic Coatings*, vol. 168, **DOI:10.1016/j.porgcoat.2022.106866**.

[18] Mohamed, H., Camdali, U., Biyikoglu, A., & Aktas, M. (2022). Enhancing the Performance of a Vapour Compression Refrigerator System Using R134a with a CuO/CeO2 Nano-refrigerant. *Strojniški vestnik - Journal of Mechanical Engineering*, vol. 68, no. 6, p. 395-410, **DOI:10.5545/sv-jme.2021.7454**.

[19] Wei, K, Yang Y, Zuo H, Zhong D.(2020). A review on ice detection technology and ice elimination technology for wind turbine. *Wind Energy*, vol. 23, p.433-457, **DOI:10.1002/we.2427**.

[20] Parent, O., Ilinca, A . (2010). Anti-icing and de-icing techniques for wind turbines: Critical review. *Cold Regions Science and Technology*, vol. 65, no. 1, p. 88-96, **DOI:10.1016/j.coldregions.2010.01.005**.

[21] Rodrigues, F.. Abdollahzadehsangroudi, M., Nunes-Pereira, J.; Páscoa, J. (2023) Recent Developments on Dielectric Barrier Discharge (DBD) Plasma Actuators for Icing Mitigation. *Actuators*, vol. 12, no. 5, **DOI:10.3390/act12010005**.

[22] Lee, S.-H., Kim, J., Seong, M., Kim, S., Jang, H., Park, H.W., Jeong, H.E. (2022). Magneto-responsive photothermal composite cilia for active anti-icing and de-icing. *Composites Science and Technology*, vol. 217, **DOI:10.1016/j.compscitech.2021.109086**.

[23] Zhang, F., Zhang, L., Li, Y., Liu, Z., Zhu, P. (2018). Experimental investigation of the icing scaling test method for a rotating cone. *Proceedings of the Institution of Mechanical Engineers, Part G: Journal of Aerospace Engineering*, vol. 233, no. 9, p. 3368-3380, **DOI:10.1177/0954410018796037**.

[24] Vertuccio, L., Foglia, F., Pantani, R., Guadagno, L. (2021). New aircraft anti/de-icing technologies. *IOP Conference Series: Materials Science and Engineering*, vol. 1024, no. 1, D**OI:10.1088/1757-899x/1024/1/012012**.

[25] Qi, L.J., Zhu, X., Zhu, C.H. (2010). YAG and CO_2 lasers. *Optical Engineering*, vol. 49, no. 11, **DOI:10.1117/1.3509366**.

[26] Gong, S.S.(2021). Simulation study on ultrasonic frequency for de-icing transmission lines. South China University of Technology, **DOI:10.27151/d.cnki.ghnlu.2021.005015**.

[27] Ding, L., Wang, X., Zhang, W., Wang, S. (2018). Study on the difference between microwave frequencies and road structure materials. *Applied Sciences*, vol. 8, no. 12, 2360, **DOI:10.3390/app8122360**.

[28] Lu, S., Kong, L.Y., Du, J. (2021). Simulation and experimental research on microwave radiation port height in road microwave de-icing. *Science Technology and Engineering,* vol. 21, no. 29, p. 12695-12703.

[29] He, Q., Li, K.S., Xu, Z.H., Wang, J.W., Wang, X.S., Li, A.L. (2023). Research progress on construction strategy and technical evaluation of aircraft icing accretion protection system. *Chinese Journal of Aeronautics,* vol.36 ,no. 10, p. 1-23. **DOI:10.1016/j.cja.2023.07.003**.

[30] Li, Y., Linwei Z, Zhiqiang H. (2023). Turbine Blades Based on Polymorphic Intelligent Network. *International Conference on Ubiquitous Communication*, p. 432-437, **DOI:10.1109/Ucom59132.2023.10257589**.

[31] Peng, Z., Hwang, J., Andriese, M., Zhang, Y., Li, G. (2016). Microwave Power Absorption Characteristics of Iron Oxides. Springer, Cham, **DOI:10.1007/978-3-319-48191-3_37**.

[32] Sarshar, M.A., Song, D., Swarctz, C., Lee, J., Choi, C.H. (2018). Anti-of Superhydrophobic Surfaces with Hierarchical Structures. *Langmuir*, vol. 34, no. 46, p. 13821-13827, **DOI:10.1021/acs.langmuir.8b02231**.

[33] Zhou, F., Zhu, J., An, N., Wang, C., Liu, J., Long, L. (2020). The anti-icing and deicing robot system for electricity transmission line based on external excitation resonant. *IEEJ Transactions on Electrical and Electronic Engineering*, vol. 15, no. 4, p. 593-600, **DOI:10.1002/tee.23093**.

[34] Palacios, J., Smith, E., Rose, J., Royer, R. (2011). Ultrasonic de-icing of wind-tunnel impact icing. *Journal of Aircraft*, vol. 48, no. 3, p. 1020-1027, **DOI:10.2514/1.C031201**.

[35] Shen, Y., Wu, X., Tao, J., Zhu, C., Lai, Y., Chen, Z. (2019). Icephobic materials: Fundamentals, performance evaluation, and applications. *Progress in Materials Science*, vol. 103, p. 509-557, **DOI:10.1016/j.pmatsci.2019.03.004**.

[36] Qi, L.J. (2012). Theoretical and experimental research on laser deicing of transmission lines. *Huazhong University of Science and Technology*, DO**I:10.7666/d.D298049**.

[37] Cheng, S.M., Guo, P., Wang, X., Che, P.D., Han, X., Jin, R.Y., Heng, L.P., Jiang, L. (2022). Photothermal slippery surface showing rapid self-repairing and exceptional. *Chemical Engineering Journal*, vol. 431, **DOI:10.1016/j.cej.2021.133411**.

[38] Wang, Y.L. (2017). *Simulation Study on Microwave De-icing in Electrified Railway Tunnels*. Southwest Jiaotong University.

[39] Liu, Z.Y., Mu, Z., Wang, J.K., Chang, Z., Liu, J. (2018). Design and parameter analysis of laser deicing optical system. *Acta Photonica Sinica*, vol. 47, no. 8, p. 147-153, **DOI:10.3788/gzxb20184708.0822001**.

[40] Pan, R., Zhang, H.J., Zhong, M.L. (2021). Triple-scale superhydrophobic surface with excellent anti-icing and icephobic performance via ultrafast laser hybrid fabrication. *ACS Applied Materials & Interfaces*, vol. 13, no. 1, p. 1743-1753, **DOI:10.1021/acsami.0c16259**.

[41] Niu, J., Jiang, W., Zou, D., Kuang, J., Liu, L., Qiao, X. (2021). Mechanical system design and motion space analysis for transmission line insulators laser de-icing robot. *Journal of Physics: Conference Series*, vol. 2002, no. 1, **DOI:10.1088/1742-6596/2002/1/012026**.

[42] Kollar, E.L., Farzaneh, M., Dyke, V.P. (2013). Modeling ice shedding propagation on transmission lines with or without interphase spacers. *IEEE Transactions on Power Delivery*, vol. 28, no. 1, p. 261-267, **DOI:10.1109/tpwrd.2012.2212918**.

[43] Kuang, J.H., Zou, D.H., Jiang, W., Liu, L.L., Peng, S.S. (2021). Research on configuration design of a suspended insulator string laser de-icing robot for UHV transmission lines. *Electric Power Science and Engineering*, vol. 37, no. 01, p. 25-32, **DOI:10.3969/j.ISSN.1672-0792.2021.01.003**. (in Chinese)

[44] Fan, S., Jiang, X., Shu, L., He, P., Liu, P., Nie, H. (2011). Dc ice-melting model for elliptic glaze iced conductor. *IEEE Transactions on Power Delivery*, vol. 26, no. 04, p. 2697-2704, **DOI:10.1109/tpwrd.2011.2156433**.

[45] Qin, C., Mulroney, A.T., Gupta, M.C. (2020). Anti-icing epoxy resin surface modified by spray coating of ptfe teflon particles for wind turbine blades. *Materials Today Communications*, vol. 22, **DOI:10.1016/j.mtcomm.2019.100770**.

[46] Zheng, J., Liu, R., Liu, D., Weng, Z., Song, G., Li, W., Wang, Z. (2023). Slippery liquid infused poroussurfaces with anti-

icing performance fabricated by direct laser interference lithography. *Progress in Organic Coatings*, vol. 175, **DOI:10.1016/j.porgcoat.2022.107308**.

[47] Minaev, I.V., Sergeev, A.N., Kubanova, A.N., Dobrovolskiy, N.M., Gvozdev, A.E., Kutepov, S.N., Maliy, D.V. (2019). History of laser development and features of its application. *Chebyshevskii Sbornik*, vol. 20, no. 4, **DOI:10.22405/2226-8383-2019-20-4-423-438**.

[48] Manikandan Rajam, P., & Nampoothiri, J. (2022). Investigation of Laser Ablative Micromachining of Al/TiB_2 Nanocomposite. *Strojniški vestnik - Journal of Mechanical Engineering*, vol. 68, no. 12, p. 735-745, **DOI:10.5545/sv-jme.2022.306**.

[49] Saravanan, K., & Thanigaivelan, R. (2021). Optimization of Laser Parameters and Dimple Geometry Using PCA-Coupled GRG. *Strojniški vestnik - Journal of Mechanical Engineering*, vol. 67, no. 10, p. 525-533, **DOI:10.5545/sv-jme.2021.7246**.

[50] Jiang, Z.X. (2022). General equation of the first law of thermodynamics for heat-work conversion process. *Journal of Huanghe S&T College*, vol. 24, no. 11, p. 6-14, **DOI:10.19576/j.issn.2096-790X.2022.11.002**. (in Chinese)

[51] Ning, Y.-p., Xu, J.-y., Huang, H., Wang, Z.-h., Yao, A., Chelladurai, S.J.S. (2022). Effect of carbon fiber admixture and length on microwave de-icing efficiency of airport road surface concrete. *Advances in Materials Science and Engineering*, vol. 2022, p. 1-14, **DOI:10.1155/2022/1956040**.